# Oxygen Activation Catalyzed by Methane Monooxygenase Hydroxylase Component: Proton Delivery during the O−O Bond Cleavage Steps†

Sang-Kyu Lee‡ and John D. Lipscomb*

*Department of Biochemistry, Molecular Biology, and Biophysics, and Center for Metals in Biocatalysis, University of Minnesota, Medical School, Minneapolis, Minnesota 55455*

*Received November 13, 1998*

ABSTRACT: The effects of solvent pH and deuteration on the transient kinetics of the key intermediates of the dioxygen activation process catalyzed by the soluble form of methane monooxygenase (MMO) isolated from *Methylosinus trichosporium* OB3b have been studied. MMO consists of hydroxylase (MMOH), reductase, and "B" (MMOB) components. MMOH contains a carboxylate- and oxygen-bridged binuclear iron cluster that catalyzes $O_2$ activation and insertion chemistry. The diferrous MMOH−MMOB complex reacts with $O_2$ to form a diferrous intermediate compound O (**O**) and subsequently a diferric intermediate compound P (**P**), presumed to be a peroxy adduct. The **O** decay reaction was found to be pH-independent within error at 4 °C ($k_{obs} = 22 \pm 2$ s$^{-1}$ at pH 7.7; $k_{obs} = 26 \pm 2$ s$^{-1}$ at pH 7.0). In contrast, the **P** formation rate was found to decrease sharply with increasing pH to near zero at pH 8.6; the observed rate constants fit to a single deprotonation event with a p$K_a = 7.6$ and a maximal formation rate at 4 °C of $k_P = 9.1 \pm 0.9$ s$^{-1}$ achieved near pH 6.5. The formation of **P** was slower than the disappearance of **O**, indicating that at least one other undetected intermediate (**P***) must form in between. **P** decays spontaneously to the highly chromophoric intermediate, compound Q (**Q**). The decay rate of **P** matched the formation rate of **Q**, and both rates decreased sharply with increasing pH to near zero at pH 8.6; the observed rate constants fit to a single deprotonation event with a p$K_a = 7.6$ and a maximal formation rate at 4 °C of $k_Q = 2.6 \pm 0.1$ s$^{-1}$ achieved near pH 6.5. No pH dependence was observed for the decay of **Q**. The formation and decay rates of **P** and the formation rate of **Q** decreased linearly with mole fraction of $D_2O$ in the reaction mixture. Kinetic solvent isotope effect values of $k_H/k_D = 1.3 \pm 0.1$ (**P** formation) and $k_H/k_D = 1.4 \pm 0.1$ (**P** decay and **Q** formation) were observed at 5 °C. The linearity of the proton inventory plots suggests that only a single proton is transferred in the transition state of the formation reaction for each intermediate. If these protons are transferred to the bound oxygen molecule, as formally required by the reaction stoichiometry, the data are consistent with a model in which water is formed concurrently with the formation of the reactive bis $\mu$-oxo-binuclear Fe(IV) species, **Q**.

The activation of $O_2$ for reaction with unactivated C−H bonds of hydrocarbons has been widely studied in the cytochrome P450 (P450)[1] family of monooxygenases (*1*−*5*). Recently, another type of oxygenase with this capability has been discovered which utilizes a non-heme iron cofactor (*6*−*10*). Typified by the soluble form of methane monooxygenase (MMO), this enzyme class binds two iron atoms in a carboxylate- and oxygen-bridged binuclear cluster in the active site. Despite the fact that P450 and MMO type monooxygenases utilize different cofactors, they still exhibit many similarities (*7*, *11*) including their reaction stoichiometry:

$$R{-}H + O_2 + NAD(P)H + H^+ \rightarrow R{-}OH + H_2O + NAD(P)^+$$

Both enzymes utilize the redox properties of iron for catalysis and initiate oxygen activation by reduction of the iron center. In the case of P450 (*2*), $O_2$ binds to the one-electron-reduced state of the heme in the enzyme, while in the case of MMO, the two-electron-reduced state of the hydroxylase component (MMOH) diiron cluster is the reactive form (*12*). As illustrated in Scheme 1, it is widely believed that P450 then accepts a second electron to yield a peroxy intermediate which undergoes heterolytic O−O bond cleavage to release water and generate an oxo-Fe(IV) porphyrin $\pi$ cation radical intermediate which is capable of attacking unactivated C−H bonds by hydrogen atom abstraction (*2*). We have speculated that because the oxy-MMOH already has been reduced by two electrons, it can undergo O−O bond cleavage directly to yield an activated oxo species (*12*−*17*). Formally, as shown in Scheme 1, this might be

† This work was supported by NIH Grant GM40466.

* To whom correspondence should be addressed at the Department of Biochemistry, Molecular Biology, and Biophysics, 4-225 Millard Hall, University of Minnesota, Minneapolis, MN 55455. Telephone: (612) 625-6454. FAX: (612) 625-2163. E-mail: lipsc001@tc.umn.edu.

‡ Current address: Department of Chemistry, Stanford University, Stanford, CA 94305.

[1] Abbreviations: D, $^2$H; KSIE, kinetic solvent isotope effect; MMO, methane monooxygenase; MMOH, MMO hydroxylase component; MMOB, MMO component B; MMOR, MMO reductase component; MOPS, 3-(*N*-morpholino)propanesulfonic acid; P450, cytochrome P450 monooxygenase; TAPS, *N*-tris[[(hydroxymethyl)methyl]-3-amino]propanesulfonic acid; **O**, **P***, **P**, **Q**, and **T**, compounds O, P*, P, Q, and T from the MMOH catalytic cycle.

10.1021/bi982712w CCC: $18.00 
Published on Web 03/17/1999

Scheme 1: Comparison of Oxygen Activation Steps in the Catalytic Cycles of Cytochrome P450 (Top) and MMO (Bottom)[a]

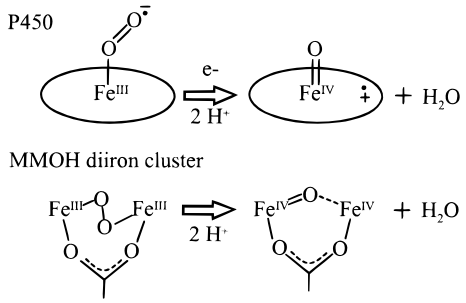


[a] This scheme is drawn to emphasize the similarity in reactant stoichiometries, oxidation state, and stabilization strategies of the respective reactive species. The actual reactive species for MMO is known to have a second single atom oxygen bridge linking the Fe(IV)s, but its origin is unknown.

considered an oxo-Fe(IV)·Fe(IV) species where the second Fe(IV) is derived from Fe(III) which has given up an electron to stabilize the oxo moiety in much the same way that the heme porphyrin macrocycle is oxidized to the radical to stabilize the reactive species in P450.

A key aspect of the reaction mechanism of monooxygenases is the delivery of the protons required by the reaction stoichiometry to generate water as a product. Heterolytic O−O bond cleavage would be facilitated if the bound $O_2$ were to be asymmetrically protonated as the bond breaks. Based on its X-ray crystal structure, $P450_{cam}$ was proposed to utilize one or more amino acid side chains and active site solvents to shuttle protons from the bulk solvent to the terminal oxygen of bound $O_2$ to promote bond cleavage (*18*−*20*). Studies of site directed mutants of $P450_{cam}$ targeted to the putative proton transport residues have generally supported this proposal (*18*, *20*−*22*). Also, solvent deuteration was observed to decrease the rate of disappearance of the initial oxy intermediate for $P450_{cam}$ due to a kinetic solvent isotope effect (KSIE) (*23*). Evaluation of the effect of progressive increase in solvent deuteration on this rate, the so-called "proton inventory" (*24*, *25*), indicated that a minimum of two protons are in flight in the transition state of the reaction. Moreover, both the magnitude of the observed KSIE and the shape of the proton inventory curve were found to be consistent with the proposed proton donors in the multistep proton-transfer process.

The reaction stoichiometry of monooxygenases requires that two protons ultimately be delivered to form a molecule of water from one of the atoms of $O_2$. However, because the intermediates in the P450 cycle following the oxy intermediate are not directly observable in transient kinetic experiments, it has not been possible to associate the proton delivery with a specific step (or steps) in the oxygen bond cleavage and activation process itself.

In contrast to P450, the mechanism of proton delivery in MMO catalysis has not been previously addressed, although structural studies show that the active site of the hydroxylase does contain Thr, Cys, and solvent which could potentially serve as proton donors during catalysis (*26*−*29*). The kinetics of the MMO catalytic cycle are unique among monooxygenases in that successive intermediates in the catalytic cycle form with progressively decreasing rates (*17*, *30*). Consequently, several intermediates accumulate to high levels and

Scheme 2: Intermediates Detected in the Reaction Cycle of MMO in the Presence of Substrates (RH)[a]

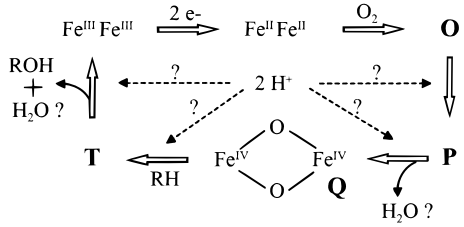


[a] The point or points of proton addition and water release are unknown and are investigated in the current study. The diferric [Fe(III)Fe(III)] and diferrous [Fe(II)Fe(II)] states of the binuclear iron cluster of MMOH are stable. The lettered intermediates have been detected, and in some cases characterized, using transient techniques.

can be trapped for further study of phenomena such as proton transfer as illustrated in Scheme 2. In the oxygen activation segment of the cycle, $O_2$ appears to first bind in the active site (but not to the diiron cluster) to form an Fe(II)·Fe(II)-containing intermediate termed compound O (**O**) (*31*). Although **O** has only been indirectly identified, the two intermediates which form spontaneously in the following steps, compounds P and Q (**P** and **Q**), have been trapped for characterization (*16*, *31*). **P** forms as $O_2$ binds directly to the Fe(II)·Fe(II) cluster with redistribution of electron density onto the oxygens to yield a putative Fe(III)·Fe(III)−peroxy complex (*30*). **Q** appears from spectroscopic studies to contain an unprecedented Fe(IV)·Fe(IV) cluster in which the irons are linked by two single atom oxygen bridges to form a "diamond core" structure (*17*, *32*). The spectroscopic studies suggest that the O−O bond of $O_2$ breaks during the **P** to **Q** conversion. Transient kinetic studies indicate that **Q** reacts directly with hydrocarbons to yield compound T (**T**), a species with hydroxylated product in the active site (*16*, *31*, *33*). The decay of **T** to release the products is the rate-limiting step in catalysis.

In light of the experiments described above for $P450_{cam}$, it is reasonable that protons enter the catalytic cycle of MMOH prior to O−O bond cleavage and formation of **Q**. However, it is also possible that **Q** is formed by a mechanism which differs from that proposed for oxygen activation by P450, and the role of the protons is to facilitate the release of both water and product at the end of the reaction. Indeed, protons might enter the reaction at any of several steps as illustrated in Scheme 2.

In the current study, we exploit the ability to resolve individual steps in the MMOH catalytic cycle to investigate the effects of solvent pH and deuteration on the rates of formation and decay of intermediates **P** and **Q**. It is found that proton delivery is likely to play a very significant role in the formation of each intermediate and thus in the oxygen activation phase of the catalytic cycle. However, the studies also suggest that the process of proton delivery differs from that described for $P450_{cam}$. These results hold significance for the understanding of both the origin of the critical activated species of the MMOH reaction cycle and the general mechanism of O−O bond cleavage by non-heme iron-containing oxygenases.

## EXPERIMENTAL PROCEDURES

*Chemicals and Standard Procedures*. All reagents were the highest grade available and were obtained from either

Sigma, Aldrich Chemicals, or EM Scientific. They were used without further purification. Water was deionized and glass-distilled or purified from deionized water using a Millipore reverse osmosis system. $D_2O$ (99.99%) was purchased from Cambridge Isotope Laboratory (Andover, MA).

*Bacterial Growth and Enzyme Preparation.* Bacterial growth of *Methylosinus trichosporium* OB3b was as reported previously (*12*). Purification of MMO was as reported previously (*12*) with minor modifications to accommodate a scaled-up process.

*Assays and Analytical Techniques.* NADH-coupled reactions were assayed either optically using nitrobenzene as a substrate or polarographically using furan as a substrate as previously described (*12, 14*). Nitrophenol concentration was determined from the absorbance at 404 nm, $\epsilon = 15$ $mM^{-1}$ $cm^{-1}$ at pH 7.7. MMOH exhibited a specific activity in the range of 800−1200 nmol $min^{-1}$ $mg^{-1}$ for furan turnover. Diiron cluster concentrations were determined by inductively coupled plasma emission spectroscopy (*12*) or colorimetric techniques. Concentrations of the protein components were determined by the method of Bradford calibrated by quantitative amino acid analysis or estimated using an extinction coefficient of 539 $mM^{-1}$ $cm^{-1}$ at 280 nm as previously described (*12*). UV−visible spectrophotometric measurements were performed using a Hewlett-Packard 8451A diode array spectrophotometer.

*Stopped-Flow Absorption Spectroscopy Experiments.* Single-turnover reactions by MMOH were monitored using a single-wavelength stopped-flow apparatus (Update Instruments or Applied Photophysics Model SX.18MV). Optical density changes were digitized and recorded using computers interfaced directly to the stopped-flow instruments. All stopped-flow experiments were performed at 4 °C except in series of experiments that included a deuterated solvent, in which case the temperature was set at 5 °C. In general, MMOH (60 $\mu$M $\approx$ 120 $\mu$M diiron cluster) and methyl viologen (10 $\mu$M) were made anaerobic in 100 mM buffer (MOPS, pH 6.5−7.9, or TAPS, pH 8−8.6) in a 3 mL conical-bottom reaction vial as previously described (*12*). A small volume of sodium dithionite in 500 mM MOPS buffer, pH 7.0, was added to stoichiometrically (2 mol of reducing equiv/mol of MMOH active sites) reduce MMOH. Then 120 $\mu$M MMOB was added anaerobically. The enzyme solution was then transferred to one stopped-flow syringe without introducing $O_2$. The second stopped-flow syringe contained air-saturated, 100 mM MOPS or TAPS buffer. After rapid mixing (1:1), absorbance changes were monitored at a fixed wavelength.

*Analysis of Transient Kinetic Data.* For all experiments, $O_2$ was added in large excess over MMOH, and MMOB was present in 2-fold excess over the MMOH concentration. Under these experimental conditions, first-order or pseudo-first-order reaction kinetics were observed. In most cases, the reactions consisted of several steps resulting in more than one exponential kinetic phase in the data. The reciprocal relaxation times and phase amplitudes of the phases were determined by nonlinear regression fitting using the program KFIT developed by Dr. Neil C. Millar (nmillar@thenet.co.uk).

*pH Profile.* Buffers used for the pH titration of the **P** and **Q** formation and decay rates were 100 mM MOPS for pH range 6.5−7.9 and 100 mM TAPS for the pH range 8.0−8.6. After rate constants were obtained by the procedures described above, the pH profiles were fitted as described under Results by a nonlinear least-squares curve-fitting program inherent in the plotting program Origin (Microcal). As a control, the experiment was also conducted using buffers in which the conductivity was normalized to that at pH 8 by adding NaCl. It was found that a maximum of 29 mM NaCl was required to adjust the conductivity of the buffers over the range specified. No differences in rates were detected as a result of this small conductivity change.

*KSIE and Proton Inventory Measurements.* The rates of **P** and **Q** formation and decay were compared in $D_2O$ and $H_2O$ and mixtures of the two solvents. Reaction progress was measured using a stopped-flow apparatus at 700 nm for **P** and at 430 nm for **Q**. Fully reduced MMOH (60 $\mu$M) was mixed with 120 $\mu$M MMOB saturated with air. The concentration of MOPS buffer used was 100 mM for both $D_2O$ and $H_2O$ stock solutions at pH(D) = 7.0, 5 °C. The pD of the buffer in $D_2O$ was adjusted using NaOD with the pH meter reading corrected by adding 0.4. Volume per volume mixtures of the stock solutions were made as appropriate for the mole fraction of $D_2O$ to be used in each experiment. The concentrated MMOH stock was directly diluted into the buffered water mixture to be used in the experiment. For experiments in which high $D_2O$ concentrations were to be used, the enzyme stock was first exchanged with $D_2O$ by three cycles of dilution/concentration using a Centricon YM-30 ultrafiltration cell followed by overnight incubation for the total exchange time of 24 h. However, it was found experimentally that MMOH equilibrated in $H_2O$ gave the same results as MMOH equilibrated in $D_2O$ when each was diluted directly into the $H_2O/D_2O$ mixture for each experiment. Rate constants for the reactions were determined as described above. The proton inventory plot was fitted as described under Results by a linear least-squares curve-fitting using Origin (Microcal). Theoretical aspects of the data analysis are treated under Discussion.

*Effects of Solvent Viscosity on Transient Kinetics.* The effects of solvent viscosity on the kinetics of **P** and **Q** formation and decay rates were examined by adding up to 25% (w/v) glycerol or 10% (w/v) sucrose to the solutions in both syringes of the stopped flow. In other respects the experiment was conducted and analyzed as described above for the case in which no viscosogen was present.

*Freeze−Quench EPR.* Reaction solutions were prepared as described for the stopped flow experiments except that higher MMOH (0.3 mM) and MMOB (0.6 mM) and $O_2$ (0 to 1.4 mM) concentrations were used. After mixing, the solution was passed continuously through calibrated aging hoses at 4 °C. The aged solutions were sprayed through a nozzle directly into an EPR tube fitted with a funnel containing isopentane at −140 °C. The sample powder was then packed tightly into the tube, and the isopentane above the sample removed while maintaining the tube at −140 °C. EPR spectra were recorded using a Varian E-109 X-band instrument equipped with an Oxford ESR-910 liquid helium cryostat. Spectra were digitally recorded and analyzed as previously described (*12*).

*Analysis of EPR Spectra.* For the analysis of EPR spectra of the ferromagnetically coupled diferrous cluster (a pair of $S = 2$ spins), the spin Hamiltonian is

$$\hat{H} = J\mathbf{S}_1\cdot\mathbf{S}_2 + \sum_{i=1}^{2}[D_i(S_{zi}^2 - 2) + E_i(S_{xi}^2 - S_{yi}^2) + \beta_e\mathbf{S}_i\cdot\mathbf{g}_i\cdot\mathbf{H}]$$

where $D_i$ and $E_i$ are the axial and rhombic zero-field splitting (ZFS) parameters and $\boldsymbol{g}_i$ are the $g$ tensors of the uncoupled sites ($i = 1, 2$). The value for $E/D$ is limited theoretically to values between 0 and $^1/_3$. Typically, the EPR spectra from integer spin systems of this type occur at high $g$-values in the range of 8−20. Simulation of the $g = 16$ signal observed from the diferrous cluster of MMOH can be used to accurately determine the absolute integer spin concentration (*34*). However, we have found that concentrations of diferrous cluster during the freeze−quench kinetic experiments can be reliably estimated by measuring the relative peak to trough intensity and normalizing to that of the fully reduced MMOH (*15*).

## RESULTS

*Effect of pH on the Decay of Diferrous MMOH after Reaction with $O_2$.* Diferrous MMOH (150 $\mu$M) in the presence of an equimolar (versus active sites) concentration of MMOB was rapidly mixed with 1.4 mM $O_2$ and frozen in isopentane at −140 °C after timed intervals using a freeze−quench apparatus. A decay rate constant for the diferrous state was determined by monitoring the $g = 16$ EPR signal characteristic of this state (*35, 36*). The pseudo-first-order rate constants were found to be 22 ± 2 $s^{-1}$ at pH 7.7, as we reported previously (*16, 31*), and 26 ± 2 $s^{-1}$ at pH 7.0, showing that this reaction has very little, if any, dependence on pH (data not shown).

*Kinetics of the Formation and Decay of **P** and **Q** at pH 7.0.* In our previous stopped-flow studies of the reaction of diferrous MMOH with $O_2$ at pH 7.7 (*16, 31*), the existence of **P** was predicted from kinetic evidence, but no direct optical evidence for this species was found. However, careful examination of the long-wavelength visible region in the current study showed that a weakly chromophoric species with a $\lambda_{max}$ at ∼700 nm (see Figure 1) forms after the decay of the $g = 16$ EPR signal from diferrous MMOH. The intermediate was then observed to convert on an even longer time scale to the strongly chromophoric intermediate **Q** ($\lambda_{max}$ at 430 nm). **P** was originally defined as the direct precursor to **Q** (*16*). The current study shows that an isosbestic point forms at 525 nm as the 700 nm species converts to **Q** (data not shown), and that the rate of decay of the 700 nm species matches the formation rate of **Q** (see below). Thus, it is reasonable to assign the 700 nm species as intermediate **P**. The characteristics of this species are similar to those of **P** (termed $H_{peroxo}$) detected during kinetic studies of *Methylococcus capsulatus* (Bath) MMOH which was reported to have a $\lambda_{max} = 625$ nm and an extinction coefficient of 1500 $M^{-1}$ $cm^{-1}$ (*30*). Fitting of the 700 nm trace of the reaction at pH 7.0 shown in Figure 1 to a three-exponential time course revealed a formation rate constant[2] of 8.0 ± 0.1 $s^{-1}$ and decay rate constants of 2.4 ± 0.2 $s^{-1}$ and 0.05 ± 0.02 $s^{-1}$. **Q** contributes somewhat to the absorbance in the 700 nm region due to the tail of its absorbance spectrum. Consequently, the rate of ∼8 $s^{-1}$ at 700 nm represents the formation rate of **P** and the rate of 2.4 $s^{-1}$ the decay rate of **P**.[3] The third and the slowest decay rate of 0.05 $s^{-1}$ probably arises from the decay of **Q** which is known to have this value at pH 7.7 (*16*). The kinetic trace of the same reaction monitored at 430 nm (where only **Q** absorbs) was fit well by summing two predominant[3] exponentials and a minor component as previously reported for the reaction monitored at pH 7.7 (*16*). From this fit, rate constants of 2.4 ± 0.1 and 0.05 ± 0.01 $s^{-1}$ were determined for the formation and decay of **Q**, respectively.

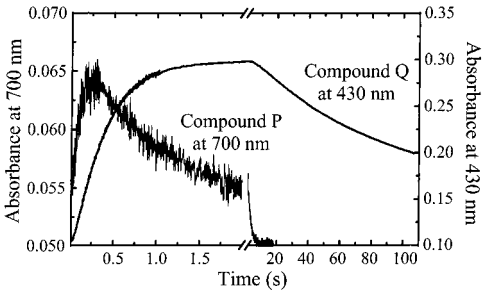


FIGURE 1: Formation and decay of **P** and **Q**. Shown are the time courses of the formation and decay reactions of **P** ($\lambda_{max}$ at 700 nm, left scale) and **Q** ($\lambda_{max}$ at 430 nm, right scale) at pH 7.0, 4 °C. A time base change for data collection was introduced at 2 s in each kinetic run. In the run shown for the **Q** time course, the integration time was increased at 1 s, causing less apparent noise in the data. The reaction conditions are described under Experimental Procedures.

The extinction coefficient of **P** can be estimated using the measured kinetic rates of **P** formation and decay. The rate constants show that at the time of maximum accumulation, **P** accounts for about 40% of the total active site concentration present and thus the estimated molar extinction coefficient of **P** determined from the total amount of MMOH present is about 2500 $M^{-1}$ $cm^{-1}$ at pH 7. This extinction coefficient value is reasonable for an iron-bound peroxo species (*38−41*). Compared with the extinction coefficient of **P** reported for MMOH from *M. capsulatus*, that found in this study is slightly higher. However, the similar Mössbauer and absorption spectra and kinetic placement in the reaction cycle suggest that the **P**s from *M. capsulatus* and *M. trichosporium* MMOHs are very similar in structure and chemical nature.

*pH Effects on the Formation and Decay Rates of **P** and **Q**.* The formation reactions of **P** and **Q** are the only steps

[2] The data are fit well to a series of summed exponentials with specific relaxation times. The number of relaxations observed defines the minimum number of steps in the reaction, but it does not define a specific mechanism or order for the steps. In the current case, rapid scan optical and time-resolved Mössbauer spectroscopies (*16, 17*) show that **P** forms prior to **Q**. If it is assumed that the steps are irreversible, then the relaxation times are equal to the reciprocal rate constants for the steps. Finally, amplitude analysis (*16*) has been used to identify which relaxation time is associated with the formation of **Q**.

[3] The time course for the formation and decay of **Q** requires a three-exponential fit as we previously reported (*16*). Two of these are apparently related to the formation of **Q** and are postulated to be due to the presence of several distinct MMOH−MMOB complexes (*15, 37*), all of which can form **Q**, but at different rates. In this study, we deal only with the faster of these exponential phases because it exhibits approximately 10-fold greater amplitude and thus appears to be the dominant process. The second phase of the **P** time course is correlated with the decay of **P** and the formation of **Q**, and consequently, must also contain a minor additional exponential component. However, in this case, we were unable to resolve it from the data.

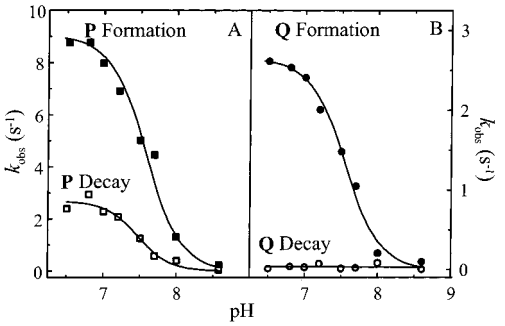


FIGURE 2: pH dependencies of the rates of **P** (A) and **Q** (B) formation and decay reactions. All reaction solutions were at 4 °C. Other conditions are given under Experimental Procedures. The data shown represent an average of three data sets with 3−5 determinations of each point within each set which gave a combined error of ±5% for each data point.

during the dioxygen activation process to show a dependency on the buffer pH. As shown in Figure 2, pH affects both the formation and decay rates of **P** in the range of pH 6.5−8.6. The pH titration data for the **P** formation rate followed at 700 nm (Figure 2A) were fitted to eqs 1 and 2 in which the formation of **P** is assumed to be irreversible and proceed from a precursor of **P**, termed **P*** (see below). The data are fit well by this procedure, indicating either that a single ionizable group is responsible for the effect or that all of the groups involved have the same p$K_a$. Also, the sigmoidal fits shown in the log plot of Figure 2 indicate that the processes follow normal (hyperbolic) saturation curves with respect to hydrogen ion concentration. This is consistent with a two-step kinetic process involving initial rapid, reversible protonation of a saturable intermediate (eq 1) as opposed to a single-step process which would not saturate. The fact that the plot extrapolates to zero velocity at high pH indicates that the second reaction in eq 1 is effectively irreversible, justifying the assumption described in footnote 2. It appears that only the protonated form of the enzyme is capable of efficiently forming **P**. The apparent p$K_a$ for **P** formation is 7.6 with an estimated maximal formation rate $k_P = 9.1 \pm 0.9$ $s^{-1}$ and an optimal pH near 6.5.

$$\mathbf{P^*} + [H^+] \overset{K_a}{\rightleftharpoons} [\mathbf{P^*}{-}H] \xrightarrow{k_p} \mathbf{P} \qquad (1)$$

$$k_{obs} = k_p \cdot 10^{(pK_a - pH)}/(1 + 10^{(pK_a - pH)}) \qquad (2)$$

The reaction could not be conducted in solutions below pH 6.5 due to precipitation of the enzyme. However, the activity of MMO remained stable for at least 30 min at room temperature in various pH buffers ranging from 6.5 to 9. Above pH 8, the rates for **P** formation and decay became very similar such that detection of **P** was difficult.

Analysis of the 430 nm data showed that only the formation rate of **Q** is sensitive to pH in the range from pH 6.5 to 8 (Figure 2B). The response of the formation rate to pH mirrored that of the **P** decay rate. The extrapolated maximal **Q** formation rate of $k_Q = 2.6 \pm 0.1$ $s^{-1}$ is achieved below pH 6.5, and a p$K_a$ value for the rate change was 7.6. Again, the assumption of a single ionization or a single p$K_a$ value for a set of ionizations allowed a satisfactory fit of the data, and a mechanistic scheme equivalent to that shown in eq 1 would be reasonable. The correlation between the decay rate curve for **P** and the formation rate curve of **Q** supports the proposed sequential formation of these species. At pH 8.0, the formation (0.2 $s^{-1}$) and decay rates (0.05 $s^{-1}$) of **Q** become comparable, leading to minimal accumulation of the intermediate.

*A New Intermediate: Compound P**. The formation rates of **P** between pH 6.5 and 8.5 are all slower than the decay rate for diferrous MMOH−MMOB. Moreover, only the former reaction exhibits a pH dependence in this pH range. This indicates that at least one more intermediate forms between these species. Previously, we have designated **O** to describe such a species (*31*). However, **O** was proposed on the basis that the decay rate of the $g = 16$ signal characteristic of the diferrous MMOH is independent of $O_2$ concentration. Hence, **O** must form as $O_2$ binds to the enzyme, but prior to the loss of the $g = 16$ signal, thereby decoupling the oxygen binding step from the observed kinetics. In the current study, we show that when the $g = 16$ signal is lost, the observed rate does not match the formation rate of **P**. Consequently, there must be one or more species between **O** and **P**. We will term this species (or set of species) compound P* (**P***), because it seems likely that it is either a diferric peroxo adduct like **P** or a mixed valent superoxo adduct based on the loss of the $g = 16$ signal characteristic of the diferrous state. While it is possible that the loss of this signal during formation of **P*** is due to a change in the coupling of ferrous ions, it seems more likely that it is caused by oxidation of one or both of the irons following association of $O_2$ with the cluster as observed for **P**.

*Kinetic Solvent Isotope Effect on Rates of P and Q*. KSIE values were measured using the proton inventory technique in which the rates of **P** and **Q** formation ($k_n$) are measured as a function of the mole fraction of deuterium in the medium ($n$) (*24, 25*).[4] Reactions were carried out at pH(D) = 7.0 where the observed rates show little change with pH. Figure 3A,B shows linear fits to the $k_n/k_H$ values for the **P** and **Q** formation rates, respectively, as a function of the mole fraction of $D_2O$. For a linear inventory plot, the KSIE can be calculated by first extrapolating to find the rate expected for 100% $D_2O$ and then forming the ratio between the rates at $n = 0$ (100% $H_2O$) and at $n = 1$ (100% $D_2O$). The observed KSIEs for **P** and **Q** formations are $k_H/k_D = 1.3 \pm 0.1$ and $k_H/k_D = 1.4 \pm 0.1$, respectively.

Previously, we have shown that exchange of protons associated with the bridging oxygen atoms of the cluster and the terminal solvent bound to the cluster of the diferric MMOH occurs very slowly, requiring over 24 h (*35, 42*). To evaluate the effects of protein deuteration or slow exchange of protons on the observed rates, MMOH was incubated in $D_2O$ for a 24 h period prior to carrying out proton inventory studies. No significant changes in the kinetic solvent isotope effects or the shape of the proton inventory plot were observed.

The ratio of the viscosities of $D_2O$ and $H_2O$ at 25 °C is 1.24 (*43*) and increases slightly to about 1.3 at 5 °C (*44*). This poses a potential source of error if the kinetics of intermediate formation are sensitive to this parameter. This possibility was examined by adding the viscosogens glycerol

[4] The KSIE studies were carried out at 5 °C since the freezing point for 100% $D_2O$ is about 3.8 °C. In previous studies, we have used a standard temperature of 4 °C. Rate differences in this temperature range were less than the error in the data and could not be distinguished.

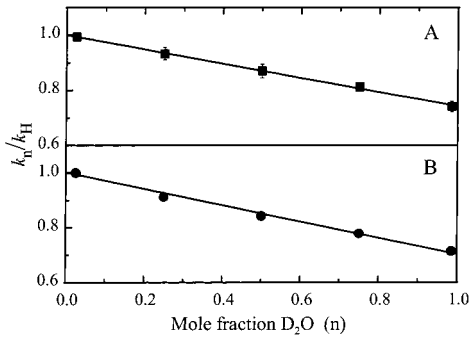


FIGURE 3: Proton inventory of **P** and **Q** formation reactions. First-order rate constants were extracted by multiexponential fitting of the reaction time course as described under Experimental Procedures. The reaction rates were followed as a function of the mole fraction of $D_2O$ in the aqueous solvent (*n*) at 5 °C. (A) **P** formation measured at 700 nm. (B) **Q** formation measured at 430 nm. The data shown are from one of three sets measured using different preparations of enzymes over a period of several months. Each set gave the same KSIE values for the **P** and **Q** reactions within error. In each data set, the kinetics at individual *n* values were measured 3−4 times for **Q** and 6−10 times for **P**. The kinetic runs were then individually fit and averaged. The standard deviation of the **Q** data was approximately the size of the symbol used. That for **P** was larger and is shown on the figure for the data points where it exceeded the size of the symbol.

Table 1: Effect of Viscosogens on the Formation Rates of **P** and **Q**[a,b,c]

| | | relative rates of formation | |
|---|---|---|---|
| viscosogen | % (w/v) | **P** (±5%) | **Q** (±3%) |
| glycerol | 0 | 1 | 1 |
| | 6.3 | 1.17 | 1.15 |
| | 12.6 | 1.63 | 1.27 |
| | 25.2 | 1.98 | 1.57 |
| sucrose | 10 | 1.42 | 1.14 |

[a] $T$ = 5 °C, pH(D) = 7.0. Other conditions are given under Experimental Procedures. [b] The decay rate of **P** mirrors the response of the formation of **Q** to viscosogens. [c] The decay rate of **Q** increases slightly over the range of glycerol used, but is unaffected by inclusion of 10% sucrose.

or sucrose to the reaction mixtures in sufficient concentration to mimic the viscosity of $D_2O$ at 5 °C (glycerol, ∼12%, sucrose ∼10%). As shown in Table 1, it was observed that both viscosogens caused similar small increases in the rates of **P** and **Q** formation. Glycerol also caused a small increase in the rate of **Q** decay which may indicate that it is a poor substrate or that it causes a minor change in MMOH structure. The increase in rates of **P** and **Q** formation is not understood, but the fact that it is consistent for two different viscosogens suggests that it may be a general effect. If so, then the true KSIE values are slightly larger than those reported here.

## DISCUSSION

The activation of dioxygen by MMO ultimately involves formation of the diamond core bis $\mu$-oxo (or equivalent) binuclear Fe(IV) species termed **Q** that is oxidized by 2 equiv relative to the putative diferric peroxy intermediate, **P** (*16, 17, 32*). Formation of **Q** could be accomplished in a single step from **P** by cleaving the O−O bond. If this bond is broken homolytically, then the diamond core of **Q** could be formed by one electron transfer to each resulting oxygen atom (formally oxygen radicals) from the Fe(III)s to yield the diferryl species. Alternatively, if the O−O bond breaks heterolytically, water and an oxygen atom would be the formal products. Release of water from the cluster and one-electron donation from each iron to the second oxygen would yield an oxo-Fe(IV)·Fe(IV) state. In this case, the formation of the diamond core would require a process such as recruitment of a solvent molecule or movement of a glutamate iron ligand to a monodentate bridging position. A key difference in these O−O bond cleavage strategies is the requirement for protons. Heterolytic cleavage with water release would be facilitated by single or double protonation of one of the oxygen atoms of the peroxy species, whereas homolytic cleavage would be favored by either no protonation or symmetrical protonation. Experimentally, the bridging oxygens of **Q** do not appear to be protonated (*32*), so if protonation occurs as part of the O−O bond breaking process, the protons either leave with the water product or leave due to deprotonation of the oxygen atoms of the diamond core in a separate, non-rate-limiting step. In this study, we show that the formation rates of the key reaction cycle intermediates, **P** and **Q**, are both pH dependent and sensitive to the solvent isotope composition.[5] This is the first direct demonstration that protons are required for the dioxygen activation phase of the catalytic cycle of MMOH. The nature of the protonation reactions and their bearing on the possible O−O bond cleavage mechanisms can be characterized in more detail through analysis of the proton inventory curve, the pH dependence, and the magnitude of the observed KSIEs. These aspects of the reaction are discussed in the following sections.

*Proton Inventory: Linear Model.* The proton inventory is described by eq 3 (*24, 25*) where $\phi_i^T$ and $\phi_j^R$ designate fractionation factors for *i*th and *j*th exchangeable proton in the transition state and the reactant state, respectively. The individual fractionation factors measure the deuterium preference of a particular site in the reactant or transition state relative to the deuterium preference for the bulk water (*24*). The term *n* is the atom fraction of deuterium in the solvent, and $k_n$ is the rate measured at that *n* value. The term $k_H$ is the rate measured in nondeuterated solvent.

$$\frac{k_n}{k_H} = \frac{\prod_{i=1}^{v}(1 - n + n\phi_i^T)}{\prod_{j=1}^{w}(1 - n + n\phi_j^R)} \quad (3)$$

When $\phi^R = 1$ for all sites involved in the reactant state, eq 3 becomes much simpler because the denominator is unity. In the reactant state, bonds formed between hydrogen and neutral oxygen or nitrogen are essentially equivalent to those between hydrogen and oxygen in bulk water. Thus, the fractionation factors for common proton donors such as

[5] Lippard and co-workers (*45*) reported the observation of a similar intermediate for the MMO isolated from *M. capsulatus* (Bath). **Q** formation from the latter system, however, shows no pH- or $D_2O$-dependent changes in either formation or decay rates (*30*). Because of the remarkable structural similarities of MMOs from these two sources, these differences in kinetics were unexpected.

hydroxyl,[6] carboxyl, and primary and secondary amine functions are effectively 1. In cases where there is an observable isotope effect, the products of the fractionation factors for the transition state and the reactant state cannot be equal. If the overall fractionation factor (i.e., the product of the individual values according to the denominator of eq 3) for the reactant state is known, then that for the transition state can be determined experimentally by fitting the proton inventory plot. Alternatively, if the fractionation factors for the reactant ($\phi^R$) and product ($\phi^P$) states as well as the extent to which the transition state has progressed toward the product ($\alpha$) are known, then the fractionation factor for the transition state can be calculated. When only a single proton is transferred, $\phi^T$ is given by eq 4.

$$\phi^T = (\phi^R)^{1-\alpha}(\phi^P)^{\alpha} \quad (4)$$

In cases where the observed KSIE arises from the contribution of a single proton in the transition state, i.e., $\phi^R = 1$ but $\phi^T \neq 1$, the proton inventory plot ($k_n/k_H$ vs $n$) will be linear as described by eq 5, and the inverse of the observed isotope effect ($k_D/k_H$) gives the value of $\phi_i^T$.

$$\frac{k_n}{k_H} = (1 - n + n\phi^T) \quad (5)$$

A simple model to account for a linear response invokes a single proton transfer during the reaction under consideration. If two or more protons are being transferred in the transition state, then the proton inventory plot is nonlinear because the numerator of eq 3 becomes a quadratic or higher function. When the value for $\phi^R \neq 1$, then both single proton-transfer and multiple proton-transfer processes give nonlinear proton inventory plots. For example, in the case of a proton transfer involving an SH group ($\phi = 0.40-0.46$) as a proton donor, the KSIE arising from the reactant state contribution would yield a nonlinear plot.

In the case of $P450_{cam}$, a nonlinear proton inventory has been observed for the second electron-transfer reaction that leads to O−O bond cleavage (*22, 23*). This is the only step in the reaction cycle that displays a significant solvent isotope effect, suggesting that this is the step in which the protonation of oxygen, required by the reaction stoichiometry, actually occurs. The authors proposed that a proton relay system delivers a proton to the distal atom of $O_2$ bound to the heme iron at the oxidation state of peroxide as part of the bond breaking process (*20, 23*). Given the shape of the proton inventory curve, it was concluded that the delivery of the proton involves two steps. Moreover, given the magnitude of the observed isotope effect (1.8) and the likely participants in proton transfer from the known structure (*21, 46, 47*), it was shown that a mechanism involving transfer of a proton from an Asp through water or Thr to the peroxy intermediate was consistent with the data. Other possibilities such as three-step transfers or simultaneous transfer of two protons to the peroxy intermediate were deemed unlikely because these processes predicted the incorrect KSIE and/or shape of the proton inventory curve.

Scheme 3: Summary of the Potential Proton Donor Groups in the Active Site of MMOH Based on the Crystal Structure of the Diferric State (*28*)

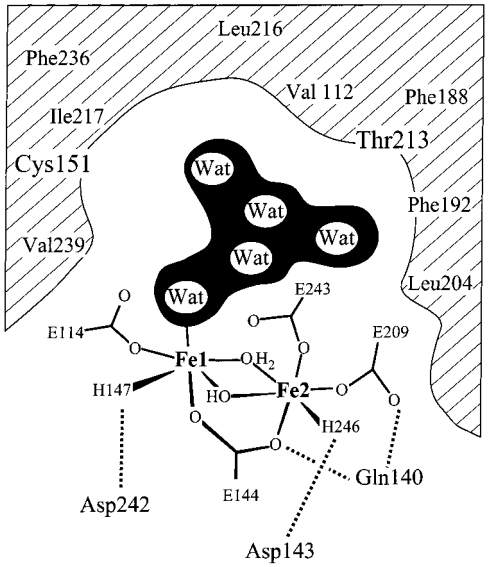


As in the case of $P450_{cam}$, the only isotope-sensitive steps in the MMOH catalytic cycle detected thus far are the formation and decay of **P** and the formation of **Q**, suggesting that these are the steps where the protons required by the reaction stoichiometry enter the cycle. However, in contrast to $P450_{cam}$, MMOH gives linear proton inventory plots for both of these oxygen activation steps. This observation significantly limits the possibilities for the participants and the chemical events in the proton-transfer process. For example, as indicated by eq 5, the linear plots rule out mechanisms similar to that of $P450_{cam}$ in which multiple steps are required to deliver a proton during the formation of **P** and **Q**. Thus, it appears that in each step a single proton is delivered by a single proton donor with a near-unity fractionation factor ($\phi^R \approx 1$).

*Potential Proton Donors.* It is possible that the proton donor reactions may occur in a part of the protein remote from the active site and transmit their effects by a conformational change. However, it seems likely that a conformational change would involve many proton-transfer events with small but finite isotope effects as hydrogen bonds are broken and formed and, therefore, result in a nonlinear proton inventory (*24*). Consequently, we favor the proposal that the proton-transfer events involve protonation of the bound oxygen, or perhaps, of nearby active site residues so that the O−O bond breaking event is directly influenced in some way.

If it is assumed that the proton-transfer reactions do occur in the active site, then there are only a few candidates for proton donor groups with fractionation factors near unity as revealed by the crystal structures of the enzyme and summarized in Scheme 3 (*27*−*29*).[7] Furthermore, only some

[6] When positive charge appears on the oxygen of the CO−H group, the fractionation factor decreases to less than unity due to weakening of the CO−H bond. For example, when the O atom of Thr is hydrogen bonded to a second proton from a solvent water, the fractionation factor for Thr−($\delta^+$)O−H is expected to be 0.69 (*24*).

[7] Scheme 3 depicts the crystal structure of the oxidized state of the enzyme. Two changes occur as the enzyme is activated. First, a complex forms with MMOB and MMOR, and second, the diiron site is reduced to the diferrous state (*8*). Either or both of these changes could cause alterations in the positions of potential proton donors.

of these residues are likely to participate in the reaction based on the characteristics reported here. Amino acid residues with near-unity fractionation factors that are within about 7 Å and show appreciable conservation among MMOs and related $O_2$-activating enzymes are limited to Asp242, Gln140, and Thr213. Of these, Gln140 is only conserved in MMOs. Typical proton donor residues such as His are not present except as iron ligands, and in this case, the residues exist in the deprotonated state. Another possible proton donor, Cys151, is located about 8 Å from the diiron cluster, but it is neither highly conserved nor does it have a fractionation factor near 1, so it can readily be discounted. Thr213 is particularly attractive because it is closest to the diiron cluster, is highly conserved among the oxygen-activating enzymes in both the P450 (*20*, *23*) and binuclear iron cluster (*26*) monooxygenase families, and would have the appropriate fractionation factor under the assumption that it is not hydrogen bonded to another proton donor. In addition to the side chain amino acid residues, the crystal structure of reduced MMOH shows that one, or possibly two, water molecule occupies a metal binding site and could potentially serve as a proton donor if it is retained in **P*** (*29*). Also, solvent molecules seen in the active site near the cluster in the crystal structure of the resting enzyme could serve as the proton donor if they are not displaced when the enzyme is reduced.

One way to select among possible donors is to use the information from the observed pH dependence for **P** and **Q** formation shown in Figure 2. These data are fit well under the assumption that the rate of the reaction for each step is controlled by the protonation state of a single group (or groups with the same p$K_a$) of about 7.6. This is consistent with this group acting as the proton donor in each step. The usual p$K_a$ values for water, Asp, Gln, or Thr are significantly different than 7.6 in the absence of hydrogen bonding. Although the solvent in the active site appears to be in a hydrogen-bonded ensemble (*28*), no such interactions are apparent for the Asp, Thr, and Gln residues found near the diiron cluster of MMOH. More importantly, if the proton donor is hydrogen bonded, then the proton-transfer reaction would probably involve more than one step, and thus it would be inconsistent with the linear proton inventory plots. In contrast, the p$K_a$ values of the metal-bound active site solvent(s) are expected to be in the appropriate range. The p$K_a$ for the water bound to mononuclear ferric ion (the redox state of the irons in **P** and possibly **P***) would be expected to be significantly lower than that for free water due to transfer of positive charge from the metal. Indeed, it has been reported to vary over a wide range (p$K_a$ = 3.7−7.6) (*48*−*50*). On the other hand, if the donor is ferric ion-bound hydroxide rather than water, the p$K_a$ will be 4−5 units higher (p$K_a$ = 7−12) (*51*). If the donor is water-associated with a ferrous ion (another possibility for **P***), a p$K_a$ in the range of 8−11 is expected (*50*). In each of these cases, the increased positive charge on the solvent oxygen would be expected to decrease the fractionation factor slightly to about 0.9 (*24*). This would, in principle, cause a slight nonlinearity in the proton inventory plot; however, it is unlikely that the small deviation would be detectable by the methods used here.

Regardless of the specific identity of the proton donors, the fractionation factors for the protons in the transition states

Scheme 4: Hypothesis To Account for the Observed Proton Inventory Plots and pH Dependencies of the P and Q Formation Reactions Which Occur during the Dioxygen Activation Phase of the MMO Catalytic Cycle[a]

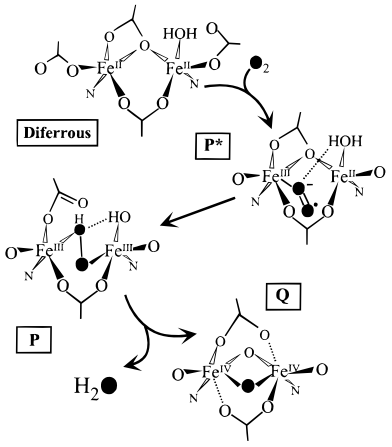


[a] The active site diiron cluster is viewed from the active site side in this scheme (opposite view from that used in Scheme 3). Filled circles represent oxygen derived from $O_2$. In this scheme, the protons are derived from metal-bound $H_2O$ which preserves the charge of the cluster, and provides a source of the second bridging oxygen for the diamond core structure of Q. However, water from the active site or the protein matrix could potentially serve as the proton donor if its p$K_a$ is decreased by other interactions. In this case, simple non-rate-limiting deprotonation of the metal-bound solvent could maintain the charge of the cluster.

of **P** and **Q** formation can be calculated using eq 5 as 0.76 and 0.70, respectively. Given that the proton donor must have a fractionation factor near unity ($\phi^R = 1$), eq 4 indicates that the proton acceptors (the product state) must have fractionation factors the same or less than the experimentally determined transition state fractionation factors. If the proton is transferred directly to a metal-bound oxygen moiety in compounds **P*** or **P**, the immediate products would be protonated, metal-bound peroxides. While the fractionation factor for peroxide in solution is close to 1, the fractionation factor for the metal-bound peroxide is not known. However, it can be substantially reduced, approaching 0.69 if positive charge is transferred from the metal to the oxygen as observed for hydrogen bond acceptor hydroxyl functions (*24*, *25*). This is in accord with the observed values for $1/\phi^T$. Also, transfer of a second proton to an already protonated intermediate (i.e., an intermediate with increased positive charge) would be expected to have a smaller fractionation factor in the transition state as observed for the **P** to **Q** reaction. It is interesting to note that studies of proton-transfer reactions to form the proposed metal-bound protonated peroxide intermediates in cytochrome *c* oxidase exhibit deuterium isotope effects of 1.4, similar to the values reported here (*52*).

*Mechanistic Implications*. From this work, we have shown that oxygen activation reactions of MMO are very sensitive to pH changes, and data have been provided that are consistent with a mechanism invoking the transfer of one proton to MMOH as each of the last two intermediates forms during the oxygen activation process. Scheme 4 summarizes one hypothesis for this mechanism. In this scheme, the diferrous MMOH reacts with $O_2$ to yield an intermediate enzyme−dioxygen complex (**O**, step not shown), and then spontaneously converts to the metal-bound superoxo (or

peroxo) species (**P***). A superoxo species is preferred for this state because we have not observed a long-wavelength chromophore shown to be characteristic of a $\mu$-peroxo moiety in studies of model compounds (*38*−*41*). The first proton transfer occurs as the formally hydroperoxo species (**P**) is formed. Subsequent transfer of a second proton then yields a transient dihydroperoxo species which rapidly leads to O−O bond cleavage and generation of the bis-$\mu$-oxo activated species (**Q**). In the mechanism shown, water resulting from O−O bond scission would dissociate from the core cluster, and the second $\mu$-oxo bridge of **Q** would be formed by a solvent associated with one of the irons. However, several other mechanistic scenarios are possible at this stage.

Although this study limits the possible proton donors to species with O−H bond fractionation factors similar to those of water, proton inventory data cannot definitively identify the donor. However, a mechanism in which metal-bound solvent, or possibly active site water if its p$K_a$ is decreased by some mechanism, serves as the donor of the protons fits all aspects of the experimental data. Proton transfer from a metal-bound solvent is attractive from the standpoint that the overall charge of the cluster would remain unchanged during the oxygen activation process. Structural studies of MMOH and several states of other iron-containing enzymes (*53*, *54*) suggest that the maintenance of the resting state charge is an important determinant of the structure of intermediates that can form during a reaction cycle. In the case of MMOH, each of the structurally characterized intermediates contains a neutral binuclear metal cluster. On the other hand, it is unclear why both proton-transfer reactions would involve a group with the same p$K_a$ if a single metal-bound solvent serves as the donor in each case. One possibility is that the redox state of the metal to which the proton donor is bound changes after the first proton transfer occurs, so that the p$K_a$ of the second transfer is maintained near to that of the first transfer. It is also possible that a metal-bound proton donor is itself reprotonated by active site solvent in a non-rate-limiting step after the first proton transfer occurs.

The results presented here make it much less likely that the O−O bond breaking reaction of MMO involves homolytic bond fissure without prior protonation. However, both homolytic cleavage occurring from a symmetrically protonated hydroperoxy intermediate and heterolytic cleavage from an asymmetrical hydroperoxy intermediate can be supported. One argument for the latter scenario derives from both EXAFS preedge studies of **Q** (*32*) and calculations of the structure of **Q** (*55*, *56*) which show that coordination numbers of the Fe(IV)s are 5 or less in the reactive species. If the proton transfer occurs from metal-bound solvent(s) followed by water release, the second single atom bridge of the diamond core could then be formed by this molecule which would effectively reduce the iron coordination number as illustrated in Scheme 4. A recent spectroscopic and electronic structural study of a cis $\mu$-1,2-peroxy diferric model complex supports this mechanistic scheme (*57*). It also seems likely that a symmetrically protonated peroxide would have a substantially reduced affinity for the metal cluster and would simply dissociate as $H_2O_2$.

In the case of $P450_{cam}$, active site Thr252 has been shown to be involved in maintaining tight coupling between NADH oxidation and substrate hydroxylation (*18*−*21*, *23*). Although site-directed mutagenesis studies using unnatural amino acids have shown that this Thr is unlikely to be the source of the proton transferred, it may act by facilitating transfer from solvent (*20*). Thr213 is located in an analogous position in the active site of MMOH (*26*). Although the current study suggests that it is also not the proton donor in the catalytic cycle, it may still play an important role by, for example, acting as a hydrogen bond acceptor for the putative hydroperoxy proton of **P** to stabilize the charge buildup during the protonation process.

This is the first study of the proton uptake events in the reaction cycle of MMO. The results show that these events are an essential part of the reaction cycle that regulates the formation rates of the key intermediates in the oxygen activation phase. As in the case of other monooxygenases, control of proton transfer appears to be important in the overall regulation of the catalytic cycle. Recently, several other binuclear iron cluster-containing enzymes have been shown to form intermediates similar to **P,** ultimately leading to O−O bond cleavage reactions (*58*−*61*). The work presented here suggests that the specific mechanisms by which these reactions occur will be strongly influenced by the proton delivery systems employed in each case. MMO seems to present an excellent system for further study of this fundamental process in oxygen activation chemistry.

## ACKNOWLEDGMENT

We gratefully acknowledge many useful discussions with Dr. Thomas C. Brunold.

## REFERENCES

1. Groves, J. T., McClusky, G. A., White, R. E., and Coon, M. J. (1978) *Biochem. Biophys. Res. Commun. 81*, 154−160.
2. McMurry, T. J., and Groves, J. T. (1986) in *Cytochrome P450 Structure, Mechanism, and Biochemistry* (Ortiz de Montellano, P. R., Ed.) pp 1−28, Plenum Press, New York.
3. Porter, T. D., and Coon, M. J. (1991) *J. Biol. Chem. 266*, 13469−13472.
4. White, R. E., and Coon, M. J. (1980) *Annu. Rev. Biochem. 49*, 315−356.
5. Mueller, E. J., Loida, P. J., and Sligar, S. G. (1995) in *Cytochrome P450 Structure, Mechanism, and Biochemistry* (Ortiz de Montellano, P. R., Ed.) pp 83−124, Plenum Press, New York.
6. Dalton, H. (1980) *Adv. Appl. Microbiol. 26*, 71−87.
7. Lipscomb, J. D. (1994) *Annu. Rev. Microbiol. 48*, 371−399.
8. Wallar, B. J., and Lipscomb, J. D. (1996) *Chem. Rev. 96*, 2625−2657.
9. Feig, A. L., and Lippard, S. J. (1994) *Chem. Rev. 94*, 759−805.
10. Wilkins, P. C., and Dalton, H. (1994) *Biochem. Soc. Trans. 22*, 700−704.
11. Ortiz de Montellano, P. R. (1991) *Methods Enzymol. 206*, 533−540.
12. Fox, B. G., Froland, W. A., Dege, J. E., and Lipscomb, J. D. (1989) *J. Biol. Chem. 264*, 10023−10033.
13. Fox, B. G., Borneman, J. G., Wackett, L. P., and Lipscomb, J. D. (1990) *Biochemistry 29*, 6419−6427.
14. Andersson, K. K., Froland, W. A., Lee, S.-K., and Lipscomb, J. D. (1991) *New J. Chem. 15*, 411−415.
15. Froland, W. A., Andersson, K. K., Lee, S.-K., Liu, Y., and Lipscomb, J. D. (1992) *J. Biol. Chem. 267*, 17588−17597.
16. Lee, S.-K., Nesheim, J. C., and Lipscomb, J. D. (1993) *J. Biol. Chem. 268*, 21569−21577.
17. Lee, S.-K., Fox, B. G., Froland, W. A., Lipscomb, J. D., and Münck, E. (1993) *J. Am. Chem. Soc. 115*, 6450−6451.

18. Imai, M., Shimada, H., Watanabe, Y., Matsushima-Hibiya, Y., Makino, R., Koga, H., Horiuchi, T., and Ishimura, Y. (1989) *Proc. Natl. Acad. Sci. U.S.A. 86*, 7823−7827.
19. Gerber, N. C., and Sligar, S. G. (1994) *J. Biol. Chem. 269*, 4260−4266.
20. Kimata, Y., Shimada, H., Hirose, T., and Ishimura, Y. (1995) *Biochem. Biophys. Res. Commun. 208*, 96−102.
21. Poulos, T. L., Finzel, B. C., and Howard, A. J. (1987) *J. Mol. Biol. 195*, 687−700.
22. Vidakovic, M., Sligar, S. G., Li, H., and Poulos, T. L. (1998) *Biochemistry 37*, 9211−9219.
23. Aikens, J., and Sligar, S. G. (1994) *J. Am. Chem. Soc. 116*, 1143−1144.
24. Schowen, R. L. (1977) in *Isotope Effects on Enzyme-Catalyzed Reactions* (Cleland, W. W., O'Leary, M. H., and Northrop, D. B., Eds.) pp 64−99, University Park Press, Baltimore.
25. Schowen, K. B. J. (1978) in *Transition States of Biochemical Processes* (Gandour, R. D., and Schowen, R. L., Eds.) pp 225−283, University Park Press, New York.
26. Nordlund, P., Dalton, H., and Eklund, H. (1992) *FEBS Lett. 307*, 257−262.
27. Rosenzweig, A. C., Frederick, C. A., Lippard, S. J., and Nordlund, P. (1993) *Nature 366*, 537−543.
28. Elango, N., Radhakrishnan, R., Froland, W. A., Wallar, B. J., Earhart, C. A., Lipscomb, J. D., and Ohlendorf, D. H.(1997) *Protein Sci. 6*, 556−568.
29. Rosenzweig, A. C., Nordlund, P., Takahara, P. M., Frederick, C. A., and Lippard, S. J. (1995) *Chem. Biol. 2*, 409−418.
30. Liu, K. E., Valentine, A. M., Wang, D. L., Huynh, B. H., Edmondson, D. E., Salifoglou, A., and Lippard, S. J. (1995) *J. Am. Chem. Soc. 117*, 10174−10185.
31. Liu, Y., Nesheim, J. C., Lee, S.-K., and Lipscomb, J. D. (1995) *J. Biol. Chem. 270*, 24662−24665.
32. Shu, L., Nesheim, J. C., Kauffmann, K., Münck, E., Lipscomb, J. D., and Que, L. (1997) *Science 275*, 515−518.
33. Nesheim, J. C., and Lipscomb, J. D. (1996) *Biochemistry 35*, 10240−10247.
34. Hendrich, M. P., Münck, E., Fox, B. G., and Lipscomb, J. D. (1990) *J. Am. Chem. Soc. 112*, 5861−5865.
35. Hendrich, M. P., Fox, B. G., Andersson, K. K., Debrunner, P. G., and Lipscomb, J. D. (1992) *J. Biol. Chem. 267*, 261−269.
36. Fox, B. G., Surerus, K. K., Münck, E., and Lipscomb, J. D. (1988) *J. Biol. Chem. 263*, 10553−10556.
37. Fox, B. G., Liu, Y., Dege, J. E., and Lipscomb, J. D. (1991) *J. Biol. Chem. 266*, 540−550.
38. Dong, Y., Yan, S., Young, V. G., Jr., and Que, L., Jr. (1996) *Angew. Chem., Int. Ed. Engl. 35*, 618−620.
39. Kim, K., and Lippard, S. J. (1996) *J. Am. Chem. Soc. 118*, 4914−4915.
40. Ookubo, T., Sugimoto, H., Nagayama, T., Masuda, H., Sato, T., Tanaka, K., Maeda, Y., Okawa, H., Hayashi, Y., Uehara, A., and Suzuki, M. (1996) *J. Am. Chem. Soc. 118*, 701−702.
41. Menage, S., Brennan, B. A., Juarez-Garcia, C., Münck, E., and Que, L., Jr. (1990) *J. Am. Chem. Soc. 112*, 6423−6425.
42. Thomann, H., Bernardo, M., McCormick, J. M., Pulver, S., Andersson, K. K., Lipscomb, J. D., and Solomon, E. I. (1993) *J. Am. Chem. Soc. 115*, 8881−8882.
43. Karsten, W. E., Lai, C.-J., and Cook, P. F. (1995) *J. Am. Chem. Soc. 117*, 5914−5918.
44. *CRC Handbook of Chemistry and Physics, 70th Edition* (1990) (Weast, R. C., Ed.) CRC Press, Boca Raton, FL.
45. Liu, K. E., Wang, D. L., Huynh, B. H., Edmondson, D. E., Salifoglou, A., and Lippard, S. J. (1994) *J. Am. Chem. Soc. 116*, 7465−7466.
46. Poulos, T. L., Finzel, B. C., Gunsalus, I. C., Wagner, G. C., and Kraut, J. (1985) *J. Biol. Chem. 260*, 16122−16130.
47. Poulos, T. L., Finzel, B. C., and Howard, A. J., (1986) *Biochemistry 25*, 5314−5322.
48. Holm, R. H., Kennepohl, P., and Solomon, E. I. (1996) *Chem. Rev. 96*, 2239−2314.
49. Bull, C., McClune, G. J., and Fee, J. A. (1983) *J. Am. Chem. Soc. 105*, 5290−5300.
50. Baes, C. F., Jr., and Mesmer, R. E. (1984) *The Hydrolysis of Cations*, Chapters 10, 12, 13, Wiley, New York.
51. Cotton A. F., and Wilkinson, G. (1972) *Advanced Inorganic Chemistry*, 3rd ed., pp 170−171, Interscience, New York.
52. Hallén, S., and Nilsson, T. (1992) *Biochemistry 31*, 11853−11859.
53. Orville, A. M., Elango, N., Lipscomb, J. D., and Ohlendorf, D. H. (1997) *Biochemistry 36*, 10039−10051.
54. Orville, A. M., Lipscomb, J. D., and Ohlendorf, D. H. (1997) *Biochemistry 36*, 10052−10066.
55. Siegbahn, P. E. M. and Crabtree, R. H. (1997) *J. Am. Chem. Soc. 119*, 3103−3113.
56. Yoshizawa, K., Ohta, T., Yamabe, T., and Hoffmann, R. J. (1997) *J. Am. Chem. Soc. 119*, 12311−12321.
57. Brunold, T. C., Tamura, N., Kitajima, N., Moro-oka, Y., and Solomon, E. I. (1998) *J. Am. Chem. Soc. 120*, 5674−5690.
58. Treffry, A., Zhao, Z., Quail, M. A., Guest, J. R., and Harrison, P. M. (1995) *Biochemistry 34*, 15204−15213.
59. Pereira, A. S., Small, W., Krebs, C., Tavares, P., Edmondson, D. E., Theil, E. C., and Huynh, B. H. (1998) *Biochemistry 37*, 9871−9876.
60. Moënne-Loccoz, P., Baldwin, J., Ley, B. A., Loehr, T. M., and Bollinger, J. M., Jr. (1998) *Biochemistry 37*, 14659−14663.
61. Broadwater, J. A., Jingyuan, A., Loehr, T. M., Sanders-Loehr, J., and Fox, B. G. (1998) *Biochemistry 37*, 14664−14671.

BI982712W